Contents lists available at ScienceDirect

Applied Catalysis B: Environmental

Porous nickel-based catalysts for combined steam and carbon dioxide reforming of methane

M.M. Danilova, Z.A. Fedorova *, V.I. Zaikovskii, A.V. Porsin, V.A. Kirillov, T.A. Krieger

Boreskov Institute of Catalysis SB RAS, Russia

ARTICLE INFO

ABSTRACT

X-ray diffraction, low-temperature nitrogen adsorption, and electron microscopy combined with energy dispersive X-ray microanalysis were used for studying the effect of synthesis conditions on the phase composition and texture of a porous nickel ribbon with a MgO underlayer and of nickel catalysts supported on it. The MgO underlayer was prepared by impregnation of a nickel ribbon with a $Mg(NO_3)_2$ solution and subsequent calcination at 550 °C in air or H_2. Catalysts were synthesized by additional supporting of nickel onto supports by its impregnation with a solution of $Ni(NO_3)_2$ or a mixture of solutions $Ni(NO_3)_2$ and $Mg(NO_3)_2$. In supported reduced catalysts (750–900 °C, H_2), the phase of nickel and the solid solution of NiO in MgO were observed. A considerable part of nickel crystallites was epitaxially bound with MgO. The nickel-based catalysts were tested in combined steam and carbon dioxide reforming of methane to synthesis gas (750 °C, $CH_4/CO_2/H_2O/N_2 = 35/23/39/3$, GHSV = 62.5 L/g h). The catalysts with the MgO underlayer completely covering the nickel ribbon showed stable activity throughout the test period (18 h). After the reaction, in these catalysts on the large crystallites of nickel ribbon, dispersed nickel crystallites (5–10 nm) epitaxially bound with MgO appeared; no carbon deposits were found in them. The resistance of these catalysts to carbonization was attributed both to the formation of nickel crystallites epitaxially bound with MgO and to the formation of the MgO underlayer that covers the nickel ribbon and prevents its contact with the reaction medium.

© 2013 Elsevier B.V. All rights reserved.

1. Introduction

Currently, combined steam and carbon dioxide reforming (SCDR) of methane to synthesis gas attracts much attention. In comparison with dry reforming of methane, the use of steam in the feed for CO_2-reforming reduces the formation of carbon [1–3]. By changing the H_2O/CO_2 ratio in the reaction feed, the H_2/CO product ratio can be controlled [1–3], and this makes it possible to produce synthesis gas with the H_2/CO ratio of about 2, which is suitable for the methanol and Fisher–Tropsch syntheses [4]. The SCDR of methane enables the production of synthesis gas from such renewable energy sources as biogas, whose main components are methane, carbon dioxide and water.

Analysis of published data shows that the main direction of development of catalysts for SCDR of methane is associated with supported nickel catalysts. Nickel catalysts are active and selective in this process and are less expensive than catalysts containing platinum group metals. The characteristic drawback of nickel catalysts is their carbonization, which leads to a decrease in their activity [1,3,5–9].

The carbonization of nickel catalysts can be diminished by the addition of promoters, such as calcium oxide [1,6,7,9], magnesium oxide [3,5,7], oxides of rare earth elements [7], and by optimization of synthesis methods [10].

The implementation of the endothermic reactions of SCDR of methane requires an intensive heat transfer from an external source into the reaction zone and the equalization of the temperature inside the catalyst bed. It means that the catalysts for these reactions must have high thermal conductivity, which can be imparted by the use of metallic supports [11,12]. A number of catalysts on such supports were tested in the steam reforming of methane: nickel composite catalyst reinforced with a stainless steel gauze [13,14], a nickel catalyst supported onto an oxide underlayer deposited on porous nickel [15], a composite nickel catalyst obtained by the capsulation of lanthanum nickelate particles in metal-ceramics [16], a nickel catalyst supported on a porous nickel plate with an underlayer of MgO [17].

According to the literature available, the use of MgO as an underlayer for the nickel catalysts is very promising: it has high thermal stability, reduces carbonization because of basic properties, and it easily forms solid solutions with NiO owing to the similarity of the structural parameters, which facilitates the formation of dispersed crystallites of reduced nickel [4,18]. A number of supported nickel catalysts with a MgO underlayer have been studied: nickel catalysts

* Corresponding author. Tel.: +7 3833269402; fax: +7 38333269402.
E-mail address: sabirova@catalysis.ru (Z.A. Fedorova).

supported on metal foams [19], porous nickel plate [17], α-Al$_2$O$_3$ [5], and Al$_2$O$_3$–SiO$_2$ [7,8].

In this paper, we reported some aspects of formation of nickel catalysts supported on a porous nickel ribbon with a MgO underlayer and the catalytic properties of obtained catalysts in the SCDR of methane to synthesis gas. The use of a catalyst support in the form of a porous nickel ribbon [20] allowed us to impart the high thermal conductivity and mechanical strength to the nickel catalysts and to produce structured catalysts.

2. Experimental

2.1. Catalyst preparation

Nickel catalysts were prepared on a 0.1 mm thick porous nickel ribbon (pNirb) obtained by rolling of a nickel powder followed by calcination at 1200 °C in a H$_2$ flow [21]. The ribbon nickel support had a specific surface area of 0.15 m^2/g and the total pore volume of ca. 0.1 cm^3/g. The MgO underlayer (6 wt.%) was prepared by impregnating the support with a Mg(NO$_3$)$_2$ solution followed by drying and then by calcination at 550 °C under air (support I) or in flowing H$_2$ (support II). The decomposition of Mg(NO$_3$)$_2$ in air is a usual method for the preparation of MgO support [5,8,19,22], but in the case of a nickel support, it can lead to loosening of the nickel surface [23,24]. Therefore, to reduce the loosening of the nickel ribbon surface, decomposition of Mg(NO$_3$)$_2$ in the case of support II was carried out in a H$_2$ flow. Catalysts I were prepared by supporting of nickel on support I via its impregnation with a Ni(NO$_3$)$_2$ solution. Catalysts II were prepared on support II via its impregnation with a mixture of Ni(NO$_3$)$_2$ and Mg(NO$_3$)$_2$ solutions. After impregnation, all the catalysts were dried and then calcined at 450 °C in a N$_2$ flow. The prepared catalysts were reduced in flowing H$_2$ at 750 °C (catalysts I) or at 900 °C (catalysts II). The content of supported nickel in the reduced catalysts was 1–5 wt.%; the content of MgO in catalysts II was 7–10 wt.%.

2.2. Characterization

The specific surface area and the pore radius distribution were determined by low-temperature nitrogen adsorption at 77 K using an ASAP–2400 (Micromeritics, USA) precision instrument. The error of the evaluation of the specific surface area did not exceed 5 rel.%. For some samples, the total pore volume and the pore radius distribution were determined using mercury porosimetry. Particle morphology was examined by scanning electron microscopy (SEM) and by transition electron microscopy (TEM) with the respective use of JSM-6460LV and JEM-2010 (JEOL Co., Japan) instruments with a lattice resolution of 0.14 nm. The energy dispersive X-ray microanalysis (EDX) of some samples was performed using an EDAX energy dispersive spectrometer with a Si(Li) detector with an energy resolution of 130 eV. Crystal faces were indexed by high resolution TEM (HRTEM) of lattice fringe images. Phase analysis was carried out using X-ray diffraction patterns taken with an ARLX'TRACT (Thermo, Switzerland) instrument (monochromatized Cu K$_\alpha$ radiation).

2.3. Catalytic activity

Catalyst activity in the SCDR of methane was evaluated by the flow method under atmospheric pressure at 750 °C using a conventional continuous flow quartz reactor with an inner diameter of 14 mm. The initial reaction mixture comprised of 35 vol.% of methane, 23 vol.% of CO$_2$, 39 vol.% of H$_2$O, and 3 vol.% of N$_2$. According to [1–3], such feed composition allows a production of synthesis gas with the H$_2$/CO ratio of about 2. The feed rate of the initial mixture was 25.0 L/h. For the catalytic activity measurements, ribbon

Table 1
Unit cell parameters of oxide phases in the samples.

Catalyst	a_{MgO} (Å)	$a_{Ni_XMg_{1-X}O}$[a] (Å)	a_{NiO} (Å)
pNirb + 6.0% MgO (I)	4.215	–	4.178
pNirb + 6.0% MgO (II)	4.219	–	–
3.0% Ni/(pNirb + 6.0% MgO)(I)	–	4.207	–
4.6% Ni/(pNirb + 6.0% MgO)(I)	–	4.205	–
1.0% Ni/(pNirb + 6.7% MgO)(II)	–	4.210	–
2.7% Ni/(pNirb + 8.6% MgO)(II)	–	4.208	–
4.0% Ni/(pNirb + 10.4% MgO)(II)	–	4.208	–
MgO	4.211[b]	–	–
NiO	–	–	4.177[c]

[a] Ni$_X$Mg$_{1-X}$O – assumed solid solution of NiO in MgO.
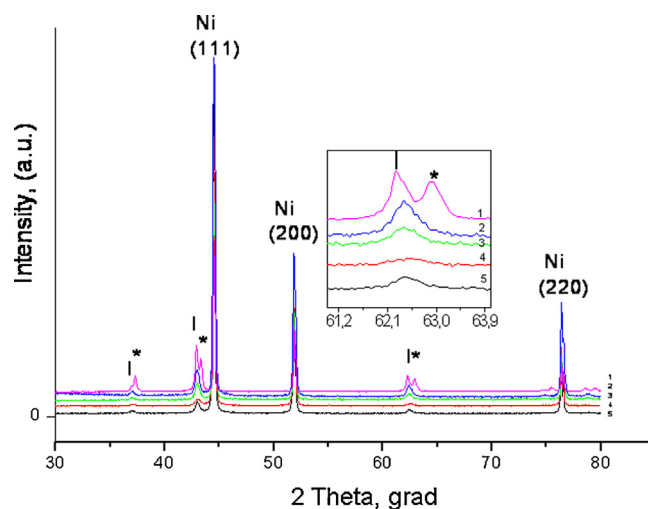[b] According to Ref. [26].
[c] According to Ref. [27].

Fig. 1. XRD pattern of samples: 1 – pNirb + 6.0% MgO (I), 550 °C, air; 2 – 4.0% Ni/(pNirb + 10.4% MgO) (II), 900 °C, H$_2$; 3 – 2.7%Ni/(pNirb + 8.6% MgO) (II), 900 °C, H$_2$; 4 – 3.0% Ni/(pNirb + 6.0% MgO), (I), 750 °C, H$_2$; 5 – 4.6% Ni/(pNirb + 6.0% MgO), (I), 750 °C, H$_2$. The insert – fragment of XRD patterns of samples. Denoted as (|) and (*) location of diffraction peaks of MgO and NiO, respectively.

catalysts were cut to pieces (1.5 mm × 1.5 mm × 0.1 mm). Catalyst samples weighing 0.40 g were used in the tests. A commercial catalyst for steam reforming of methane NIAP-18 (10.5 wt.% Ni/Al$_2$O$_3$) [25] was used for the comparison. The catalyst sample weighing 0.40 g was tested in the form of a 0.25–0.50 mm fraction. Before the activity measurements, the samples were reduced at 750 °C in flowing H$_2$. Then the reaction mixture was substituted for hydrogen and measurements were taken after keeping the catalysts in the reaction mixture for 1 h. The catalyst bed temperature was controlled with a thermocouple mounted in the reactor at the level with the catalyst bed. The temperature evaluation error was ±2 °C. The composition of reaction mixtures was analyzed chromatographically with an error less than 10%.

Catalytic activity measurements in the empty reactor showed that the methane conversion in this case was less than 1%.

3. Results and discussion

3.1. Phase composition and texture of initial catalysts

X-ray diffraction data showed that the metallic support contains only the nickel phase, whereas support I additionally contains phases of NiO and MgO with the unit cell parameter $a = 4.215$ Å (Table 1). Diffraction peaks of the oxide phases are very weak compared with the diffraction peaks of nickel (Fig. 1). In addition,

Table 2
Texture parameters of the catalysts.

Catalyst	S_{sq} (m^2/g)	D_{Ni} (nm)[a]
pNirb + 6.0% MgO (I)	0.9	–
pNirb + 6.0% MgO (I)^2	1.2	–
pNirb + 6.0% MgO (II)	7.5	–
pNirb + 6.0% MgO (II)^2	7.2	–
3.0% Ni/(pNirb + 6.0% MgO) (I)[b]	1.7	5–10
4.6% Ni/(pNirb + 6.0% MgO) (I)[b]	2.0	5–15
1.0% Ni/(pNirb + 6.7% MgO) (II)[c]	1.7	3–5
2.7% Ni/(pNirb+ 8.6% MgO) (II)[c]	1.6	3–5
4.0% Ni/(pNirb + 10.4% MgO) (II)[c]	1.9	3–7

[a] Dominant nickel particle size on the MgO surface according to TEM data.
[b] The samples were reduced at 750 °C, H$_2$.
[c] The samples were reduced at 900 °C, H$_2$.

support I contains trace amounts of the MgO precursor phase, apparently magnesium hydroxonitrate, which is indicated by corresponding, very weak, diffraction peaks. Support II contains phases of nickel and MgO with a = 4.219 Å. In the reduced catalysts with supported nickel, the diffraction peaks correspond to only one oxide phase and nickel. Diffraction peaks of the oxide phase have an interjacent position between the peaks of pure oxides and are shifted to the diffraction peaks of MgO. According to [28], this diffraction pattern indicates the formation of a solid solution of NiO in MgO. The presence of a phase of the solid solution after reduction treatment (750–900 °C, H$_2$) can be explained by hindered reduction of Ni^{2+}-cations embedded into the lattice of hardly reducible MgO (the heat of formation of MgO is higher than that of NiO [29]). An increase in the temperature of NiO reduction after the formation of its solid solution in MgO is shown in [8,18,30].

The ribbon nickel support has a macroporous structure with a low total pore volume: according to the mercury porosimetry data, most pores have the radius from 5 to 60 μm. The macroporous nature of the support is confirmed by SEM data: the support has a corpuscular structure formed by rounded nickel particles with a size of 3–30 μm fused at the contact points.

According to SEM data, the MgO underlayer forms a loose porous layer with a thickness of 2–3 μm. According to the low-temperature nitrogen adsorption data, the specific surface area of support II is 7.5 m^2/g. The MgO underlayer in support II has fine pores with an average diameter of 4–6 nm. The use of air instead of H$_2$ (support I) leads to a decrease in the fraction of fine pores and in the specific surface area (down to 0.9 m^2/g) (Table 2). The observed differences in the specific surface area of supports I and II can be explained as follows: incomplete decomposition of Mg(NO$_3$)$_2$ under air compared with its annealing in flowing hydrogen during relatively short period [31]; the formation in a hydrogen flow of a surface structure with a higher degree of defects; and the hampered sintering of MgO particles in hydrogen because of a sharper decrease in the concentration of water vapor in the pores because of the high rate of hydrogen diffusion.

As follows from the TEM images obtained, the MgO underlayer in supports I and II consists of aggregates 50–300 nm in size formed by primary 2–10-nm particles. The MgO underlayers do not contain separate nickel particles except for the sparse large (100 nm) particles probably detached from the nickel support during the sample preparation. Nevertheless, the EDX-spectra of MgO in supports I and II show Ni in the form of weak spectral lines corresponding to the Ni content not exceeding 2 at.% relative to Mg. The intensities of the nickel lines in the EDX spectra from different areas of the MgO surface are different, which indicates that during calcination, MgO non-uniformly interacts with the NiO film. Probably, the adjoined particles of MgO and NiO (Fig. 2) react to form a surface solid solution, whereas the particles of MgO that are not in contact with the surface of nickel ribbon do not contain dissolved nickel. The possibility of interaction of NiO with MgO during heating in
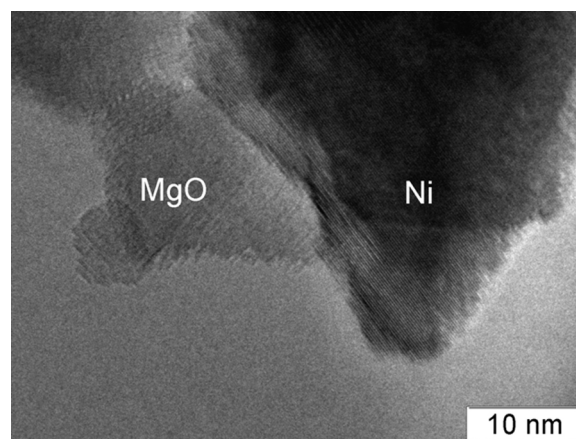

Fig. 2. HRTEM image of the nickel ribbon with MgO underlayer (support II), 550 °C, H$_2$.

hydrogen at temperatures of 250–400 °C is shown in [32], where the authors assumed that the diffusion of Ni^{2+}-cations into the surface layer of MgO proceeds in parallel with their reduction. The same assumption can be made on the basis of the data in [33]. In addition, the calcination of the impregnated nickel support leads to the decomposition of Mg(NO$_3$)$_2$ with the formation of nitrogen oxides, which are able to oxidize some parts of the nickel ribbon surface.

Impregnation of the nickel ribbon with a weak acid solution of Mg(NO$_3$)$_2$ (pH = 5.8), with the subsequent drying and calcination, may be accompanied by corrosion of nickel with the transition of Ni^{2+}-cations into solution. These cations can be incorporated into the bulk of MgO particles.

The specific surface areas of reduced catalysts on supports I and II vary to a lesser extent than the specific surface areas of the supports themselves (Table 2). This lesser difference may be due to rehydration of a substantial part of MgO during the impregnation with aqueous solutions of nitrates [34,35] and due to the partial sintering of MgO during the reduction of catalyst II at 900 °C. According to the TEM data, supported nickel particles in catalysts II have the smaller predominant size and a more uniform size distribution than those in catalysts I (Table 2).

TEM data indicate that in reduced catalysts I and II, crystallites of supported nickel are epitaxially bound with MgO (Fig. 3): the images of nickel particles exhibit a moire fringe pattern in the form of parallel fringes with a period of about 1 nm as a result of lattice spacing d_{111} of Ni and MgO superposition [36]. In catalysts II, epitaxially unbound crystallites of supported nickel are very rare; catalysts I contain nickel crystallites with the size over 15–20 nm, which are not epitaxially bound. These crystallites are oxidized and their surface contains a 1–2-nm layer of NiO. In catalysts I and II, the epitaxially bound highly dispersed (less than 7 nm) nickel crystallites do not have the oxide layer after exposure to air (Fig. 3b) [17,19]. Presumably, the surface of highly dispersed crystallites of nickel is not oxidized due to epitaxial binding of nickel crystallites with MgO. It is possible that in these crystallites, nickel is partially oxidized by the surface oxygen ions of MgO, the nickel lattice being epitaxially bound with it. As a consequence, the electron density is shifted toward the underlayer [4,37–39]. The crystallites have the structure $Fm3m$ of metallic nickel, but the induced positive charge ($\delta^+ < 2$) prevents the oxidation of the surface and the formation of the phase of NiO. According to [40], the formation of the partially reducible solid solution of NiO in MgO increases the stability of Ni—Ni bonds on the reduced surfaces. This higher surface stability prohibits nickel surface reconstruction via bond relaxation.
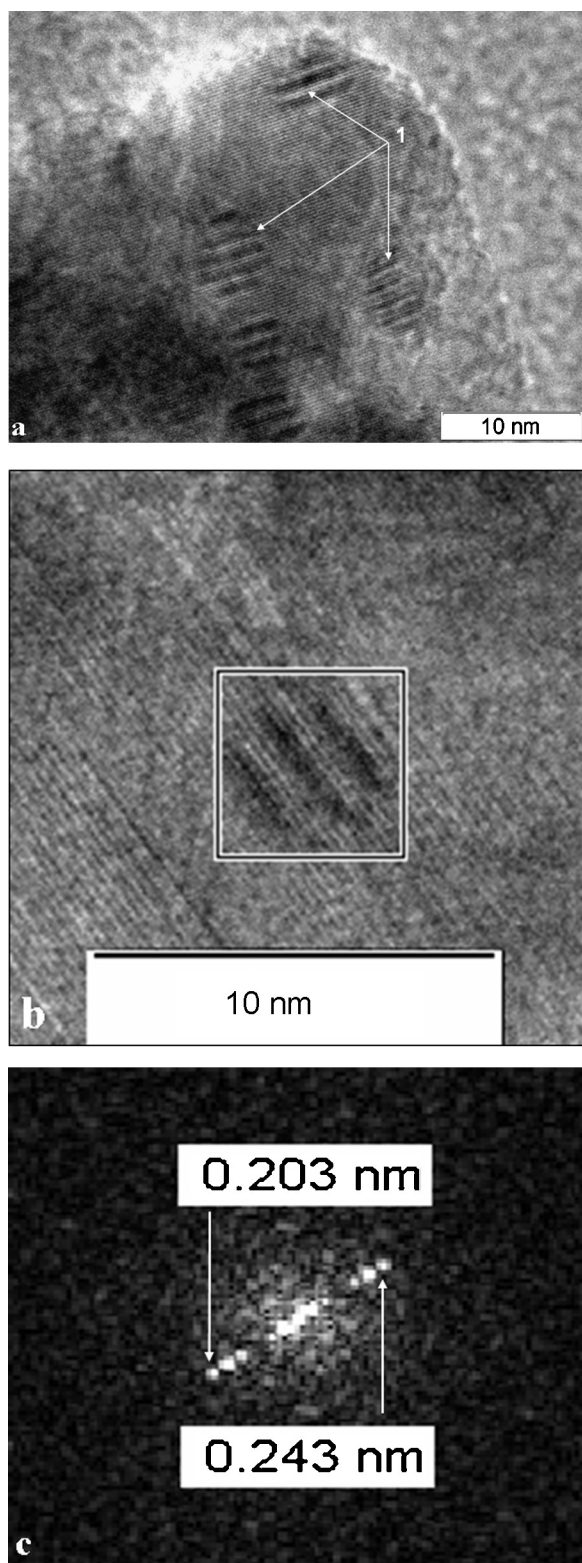
Fig. 3. HRTEM image of the catalyst 4.0% Ni/(pNirb + 10.4% MgO) (II), 900 °C, H$_2$: (a) dispersed nickel crystallites epitaxially bound with MgO (denoted as 1); (b) highly dispersed nickel crystallite without oxide layer on its surface; (c) digital diffraction pattern from this crystallite, reflections for $d_{111} = 0.203$ nm (Ni) and $d_{111} = 0.243$ nm (MgO) are shown.

It is believed that in the studied catalysts, epitaxial binding of nickel crystallites with MgO is due to the formation of nickel crystallites from a solid solution of Ni$_X$Mg$_{1-X}$O and due to their high dispersion.
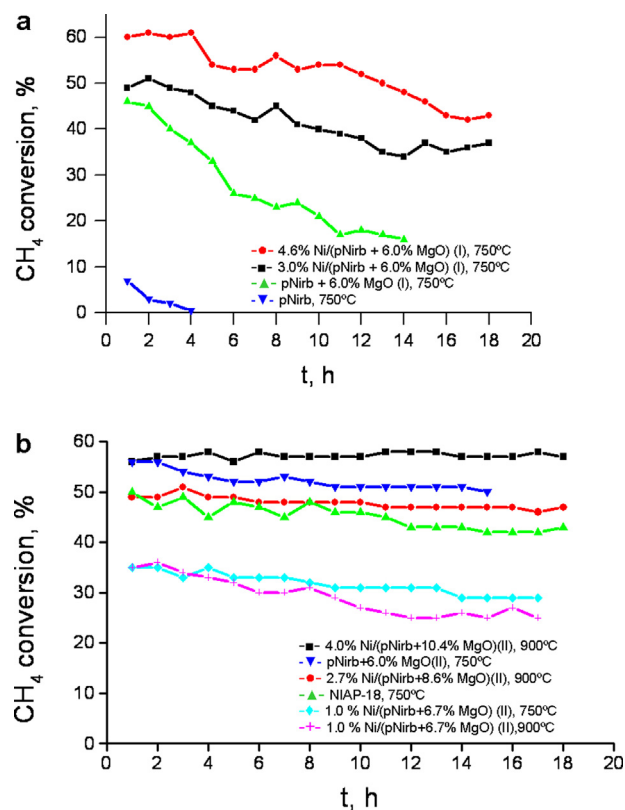

Fig. 4. Methane conversion versus time-on-stream in the steam-CO$_2$ reforming of methane over the catalysts reduced in H$_2$.

3.2. Catalytic activity

Fig. 4 shows the activity of the prepared catalysts in the SCDR of methane. The conversion of methane over the initial nickel support was 7% and decreased to 0.5% during the reaction, apparently because of carbonization. The supporting of the MgO underlayer increases the conversion of methane to 49% (support I) and 56% (support II). The increase in conversion can be attributed to the interaction of NiO and MgO with the formation of the surface solid solution, from which dispersed nickel crystallites are formed during the reduction in hydrogen or under the influence of the reaction medium [17]. The increase in activity is also facilitated by loosening of the nickel support surface during the oxidation treatment (heating in air and/or in the presence of nitrogen oxides) and subsequent reduction in hydrogen [23,24]. The higher activity of support II (compared with support I) is probably related to the higher dispersion of nickel crystallites formed from the hardly reducible solid solution under the influence of the reaction medium [17]. During the reaction, the conversion on supports I and II decreases; a sharp fall in activity over support I can be caused by sintering of the loosened nickel ribbon and by its carbonization.

Additional supporting of nickel onto supports with the MgO underlayer increases the catalytic activity (Fig. 4). With the increase in the content of supported nickel, the catalyst activity increases, which may result from an increase in the surface area of metallic nickel per unit weight of the catalyst.

Fig. 4 shows the effect of test duration on the conversion of methane. The decrease in the activity of catalysts I was about 25% and that of catalyst II containing 1.0% Ni/pNirb + 6.7% MgO was about 20%. For comparison, Fig. 4b depicts the activity of the latter catalyst but reduced at 750 °C. The decrease in the activity of the catalysts reduced at 750 and 900 °C was comparable. The activity of

catalysts II with high content of MgO (8.6 and 10.4 wt.%) remained stable throughout the test period.

The H_2/CO ratio in the reaction products over catalysts I and over catalyst II with low content of MgO (6.7 вес.%) was 2.7–2.8, whereas for catalysts II with high content of MgO, this ratio was 2.1–2.2 and almost did not change during the reaction.

For comparison, Fig. 4b presents the effect of test duration on the conversion of methane over a commercial catalyst NIAP-18. These results show that catalysts II with high content of MgO on the highly thermally conductive support are comparable in activity with the catalyst NIAP-18 and surpass it in stability under conditions of SCDR of methane.

3.3. Texture of catalysts after tests in SCDR of methane

TEM data show that after the tests in catalysts I and II, a small number of enlarged nickel crystallites (30–50 nm) appear on the MgO surface, which are evidently formed because of the partial sintering of nickel crystallites weakly bound with the underlayer. However, most of the supported nickel crystallites remain in the stable state of dispersed crystallites epitaxially bound with MgO. Some of these crystallites do not have the oxide film on their surface. Besides, there appear highly dispersed nickel crystallites (2–3 nm) epitaxially bound with MgO. In catalysts II with the high content of MgO, on large nickel particles (∼100 nm) detached from the nickel support, there appear nickel crystallites of 5–10 nm in size epitaxially bound with MgO probably containing NiO (Fig. 5a and b). In initial catalysts I and II these crystallites were not found; also they were absent in spent catalysts I and in spent catalyst II with low content of MgO. These results indicate that in catalysts II with high content of MgO under the influence of the reaction medium, there proceeds a reduction of nickel oxide from the hardly reducible solid solution NiO–MgO, which is formed on the surface of the nickel ribbon. In these catalysts, the formation of the surface solid solution is facilitated both by the supporting of nickel from a mixture of $Ni(NO_3)_2$ and $Mg(NO_3)_2$ solutions and by treatment in hydrogen at 900 °C, which increases the diffusion mobility of cations and intensifies the incorporation of Ni^{2+}-cations into the lattice of MgO and Mg^{2+}-cations into the lattice of NiO. The treatment under reaction conditions of catalysts I and of catalyst II with low content of MgO does not result in the formation of carbon on dispersed nickel crystallites epitaxially bound with MgO. However, the islet formation of graphite-like carbon was observed on the large particles of nickel (∼100 nm) detached from the nickel support. It is known [18,28,41] that large nickel particles are more prone to carbonization than small ones. As shown in Fig. 2, some parts of the nickel ribbon surface do not contact the particles of MgO. Because nickel in catalysts I was supported without the use of $Mg(NO_3)_2$, and because the content of MgO in catalyst II (1.0 wt.% Ni/pNirb + 6.7% MgO) was increased insignificantly, one can suppose that some parts of the nickel support surface can be free from the MgO underlayer. When exposed to the reaction medium, these parts can be carbonized. Thus, the observed decrease in the activity of catalysts I and of catalyst II with low content of MgO can be attributed to the carbonization of large crystallites of the nickel support that are not covered with MgO.

Catalyst II with high content of MgO exhibited stable activity and contained no carbon deposits after reaction. Their resistance to carbonization is possibly a result of the formation of dispersed nickel crystallites epitaxially bound with MgO, as well as result of the formation of the MgO underlayer, which covers completely the nickel ribbon and prevents the contact of the reaction medium with large nickel crystallites and thus prevents their carbonization. It is known [1,3,5–9] that during the SCDR of methane, nickel catalysts are inclined to carbonization. The tests of our catalysts showed that no carbon is deposited on nickel crystallites epitaxially bound with
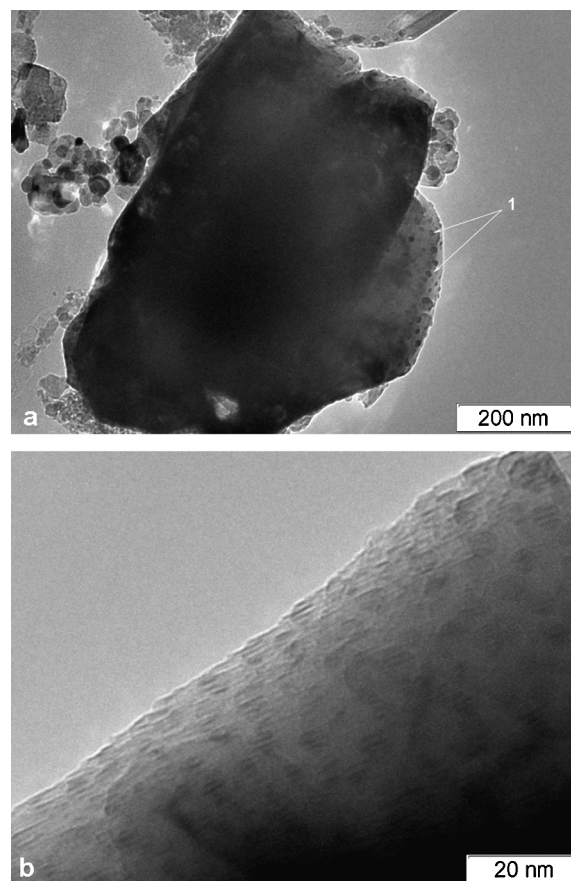

Fig. 5. TEM image of the catalyst 4.0% Ni/(pNirb + 10.4% MgO) (II) tested in the steam-CO_2 reforming of methane: (a) Ni particle from the nickel support with the dispersed nickel crystallites appeared after the reaction (denoted as 1); (b) HRTEM image of the dispersed nickel crystallites epitaxially bound with MgO (the fragment of the image (a)).

MgO. In our catalysts, a considerable part of supported nickel crystallites is formed during the reduction of the solid solution of NiO in MgO (Table 1). It can be supposed that there is the interaction of these crystallites with MgO. The interaction of dispersed nickel crystallites with MgO can be indicated by their epitaxial binding and by the absence of the oxide layer on their surface (Fig. 3). In this case, the catalytic properties of the catalyst are no longer determined only by supported metal, but refer to a unified system "metal-support" and depend on the nature of the support and the nature of its interaction with the metal [42,43]. It is believed that the epitaxial binding of nickel with MgO leads to a change in the catalyst properties and suppresses its activity in the reactions leading to the formation of carbon [44].

An increased resistance to carbonization of the catalysts in the case when the precursor of the active component is a solid solution of NiO in MgO is shown in [4,28,30,45]. It is supposed that the carbon deposition is suppressed due to the formation of highly dispersed crystallites of nickel that are in interaction with MgO [4,25,38]. According to [40], the formation of the partially reducible solid solution of NiO in MgO increases the stability of Ni–Ni bonds on the reduced surfaces; this higher surface stability inhibits carbon diffusion into the nickel lattice, and thus prevents the formation of carbon. We would like to mention that no epitaxial binding of the dispersed nickel crystallites with MgO in Ni/MgO catalysts was observed [4,9,18,22,28,45,46].

Resistance to carbonization may also increase because of the basic properties of the surface of MgO: owing to the presence of

labile hydroxyl groups [47–49] and activated molecules of CO_2 [50], which oxidize hydrocarbon fragments.

4. Conclusion

In the nickel catalysts supported on a porous nickel ribbon with the MgO underlayer, the predominant part of nickel crystallites is epitaxially bound with MgO and some of the dispersed nickel crystallites do not have an oxide film on their surface. It is believed that the epitaxial binding of nickel with MgO leads to a change the catalyst properties and suppresses its activity in the reactions leading to the formation of carbon. When tested in the SCDR of methane, the catalysts with the MgO underlayer completely covering the nickel ribbon exhibit a stable activity. After reaction, in these catalysts on the large crystallites of the nickel ribbon, dispersed nickel crystallites (5–10 nm) epitaxially bound with MgO appear; no carbon deposits are found in them.

The formation of dispersed nickel crystallites epitaxially bound with MgO and the formation of the MgO underlayer, which covers the nickel ribbon, prevents its contact with the reaction medium and thus prevents its carbonization, can determine the stability of these catalysts.

Acknowledgement

References

[1] V.R. Choudhary, A.M. Rajput, Ind. Eng. Chem. Res. 35 (1996) 3934–3939.
[2] V.R. Choudhary, K.C. Mondal, Appl. Energy 83 (2006) 1024–1032.
[3] H.-S. Roh, K.Y. Koo, J.H. Jeong, Y.T. Seo, D.J. Seo, Y.S. Seo, W.L. Yoon, S.B. Park, Catal. Lett. 117 (2007) 85–90.
[4] M.C.J. Bradford, M.A. Vannice, Catal. Rev. Sci. Eng. 416 (1999) 1–42.
[5] J. Mehz, K.J. Jozani, A.N. Pour, Y. Zamani, React. Kinet. Catal. Lett. 75 (2002) 267–273.
[6] O. Yamazaki, T. Nozaki, K. Omata, K. Fujimoto, Chem. Lett. 21 (1992) 1953–1954.
[7] V.R. Choudhary, B.S. Uphade, A.S. Mamman, Catal. Lett. 32 (1995) 387–390.
[8] V.R. Choudhary, B.S. Uphade, A.S. Mamman, Appl. Catal. A: Gen. 168 (1998) 33–46.
[9] K. Tomishige, Y. Himeno, O. Yamazaki, Y. Chen, K. Fujimoto, Kinet. Catal. 40 (1999) 432–439 (in Russian).
[10] K. Takanabe, K. Nagaoka, K. Nariair, K. Aika, J. Catal. 230 (2005) 75–85.
[11] M. Sheng, H. Yang, D. Cahela, B.J. Tatarchuk, J. Catal. 281 (2011) 254–262.
[12] T. Boger, A.K. Herbel, Chem. Eng. Sci. 60 (2005) 1823–1835.
[13] V.A. Kirillov, N.A. Kuzin, A.V. Kulikov, S.I. Fadeev, A.B. Shigarov, V.A. Sobyanin, Teor. Osn. Khim. Tekhnol. 37 (2003) 300–308.
[14] M.M. Danilova, Z.A. Sabirova, N.A. Kuzin, V.A. Kirillov, N.A. Rudina, E.M. Moroz, A.I. Boronin, Kinet. Catal 48 (2007) 121–131 (in Russian).
[15] Z.R. Ismagilov, B.B. Pushkarev, N.A. Koryabkina, H. Veringa, Chem. Eng. J. 82 (2001) 262–355.
[16] Yu.V. Potapova, Cand. Sci. (Chem.) Dissertation, Boreskov Inst. of Catalysis, Novosibirsk, 2002.
[17] Z.A. Sabirova, M.M. Danilova, V.I. Zaikovskii, N.A. Kuzin, V.A. Kirillov, T.A. Krieger, V.D. Meshcheryakov, N.A. Rudina, O.F. Brizitskii, L.N. Khrobostov, Kinet. Catal. 49 (2008) 449–456 (in Russian).
[18] Y.H. Hu, E. Ruckenstein, Catal. Rev. Sci. Eng. 44 (2002) 423–453.
[19] A. Shamsi, J.J. Spivey, Ind. Eng. Chem. Res. 44 (2005) 7298–7305.
[20] V.A. Kirillov, Z.A. Fedorova, M.M. Danilova, et al., Appl. Catal A.: Gen. 401 (2011) 170–175.
[21] G.F. Tikhonov, L.A. Pyryalov, V.K. Sorokin, Powder Metall. 12 (1973) 85–89 (in Russian).
[22] G. Chen, K. Tomishige, K. Fujimoto, Appl. Catal. A: Gen. 161 (1997) 11–17.
[23] I.M. Bodrov, L.O. Apel'baum, M.I. Temkin, Kinet. Catal. 5 (1964) 696–705 (in Russian).
[24] L.J.I. Coleman, E. Croiset, W. Epling, M. Fowler, R.R. Hudgins, Catal. Lett. 128 (2009) 144–153.
[25] V.I. Yagodkin, YuT. Fedyukin, V.N. Men'shov, V.A. Daut, Khim. Prom-st. 2 (2001) 7–12.
[26] JCPDS Data, File No. 45-0946.
[27] JCPDS Data File No. 47-1049.
[28] Y.H. Hu, E. Ruckenstein, Catal. Lett. 43 (1997) 71–77.
[29] Handbook of Chemistry, Vol. 1, Khimiya, Leningrad, 1971, pp. 786 (in Russian).
[30] O. Yamazaki, K. Tomishige, K. Fujimoto, Appl. Catal. A: Gen. 136 (1996) 49–56.
[31] T.V. Rode, Kislorodnye soedineniya khroma i khromovye katalizatory (Oxygen-Containing Chromium Compounds and Chromium Catalysts), Akad. Nauk SSSR, Moscow, 1962, pp. 184 (in Russian).
[32] G.C. Bond, S.P. Sarsam, Appl. Catal. A: Gen. 38 (1988) 365–377.
[33] N. Takezawa, H. Terunuta, M. Shimokawabe, H. Kobayashi, Appl. Catal. A: Gen. 23 (1986) 291–298.
[34] M.A. Aramendia, V. Boran, C. Jimenez, Appl. Catal. A: Gen. 244 (2003) 207–214.
[35] E. Hillerova, Z. Vit, M. Zdrazil, Appl. Catal A: Gen. 118 (1994) 111–125.
[36] P.B. Hirsch, A. Howie, R.B. Nickolson, et al., Electron Microscopy of Thin Crystals, Butterworths, 1965.
[37] M.B. Kuzminsky, A.A. Bagatur'yants, Achievements of Science and Technology, in: Series Kinetics and Catalysis, Vol. 8, VINITI, Moscow, 1980, pp. 99–181 (in Russian).
[38] E. Ruckenstein, Y.H. Hu, Appl. Catal. A: Gen. 133 (1995) 149–161.
[39] S. Tang, J. Lin, K.J. Tan, Catal. Lett. 51 (1998) 169–175.
[40] M.C.J. Bradford, M.A. Vannice, Appl. Catal. A: Gen. 142 (1996) 73–96.
[41] K. Tomishige, G. Chen, K. Fujimoto, J. Catal. 181 (1999) 91–103.
[42] L.M. Plyasova, T.M. Yurieva, T.A. Krieger, O.V. Makarova, V.I. Zaikovskii, L.P. Solovyeva, A.N. Shmakov, Kinet. Catal. 36 (1995) 464–472.
[43] G.K. Boreskov, Theoretical Problems of Catalysis, USSR Academy of Sciences, Siberian Branch, Institute of Catalysis, Novosibirsk, 1977, pp. 113–133.
[44] A.R. Kaul, O.Yu. Gorbenko, A.A. Kamenev, Russ. Chem. Rev. 73 (2004) 932–953.
[45] Y. Chen, K. Tomishige, K. Yokogama, K. Fujimoto, J. Catal. 184 (1999) 479–490.
[46] N. Nurunnbai, Y. Mukainakano, S. Kado, B. Li, K. Kunimori, K. Suzuki, K. Fujimoto, K. Tomishige, Appl. Catal. A: Gen. 299 (2006) 145–156.
[47] J. Wei, E. Iglesia, J. Catal. 224 (2004) 370–383.
[48] K. Polychronopoulou, C.N. Costa, A.M. Estaphiou, Catal. Today 112 (2006) 89–93.
[49] J.M. Aparicio, J. Catal. 165 (1997) 262–274.
[50] G.S. Gallego, C. Baliot-Dupeyrat, J. Barrault, E. Florer, F. Mondragon, Appl. Catal. A: Gen. 334 (2008) 251–258.